Vortex precession dynamics in general radially symmetric potential traps in two-dimensional atomic Bose-Einstein condensates

P. G. Kevrekidis,[1] Wenlong Wang,[2,*] R. Carretero-González,[3,†] D. J. Frantzeskakis,[4] and Shuangquan Xie[5]
[1]*Department of Mathematics and Statistics, University of Massachusetts Amherst, Amherst, Massachusetts 01003-4515, USA*
[2]*Department of Physics and Astronomy, Texas A&M University, College Station, Texas 77843-4242, USA*
[3]*Nonlinear Dynamical Systems Group, Computational Sciences Research Center, and Department of Mathematics and Statistics, San Diego State University, San Diego, California 92182-7720, USA*
[4]*Department of Physics, National and Kapodistrian University of Athens, Panepistimiopolis, Zografos, 15784 Athens, Greece*
[5]*Department of Mathematics and Statistics, Dalhousie University, Halifax, Canada B3H 3J5*
(Received 21 June 2017; published 13 October 2017)

We consider the motion of individual two-dimensional vortices in general radially symmetric potentials in Bose-Einstein condensates. We find that although in the special case of the parabolic trap there is a logarithmic correction in the dependence of the precession frequency ω on the chemical potential μ, this is no longer true for a general potential $V(r) \propto r^p$. Our calculations suggest that for $p > 2$, the precession frequency scales with μ as $\omega \sim \mu^{-2/p}$. This theoretical prediction is corroborated by numerical computations, not only at the level of spectral (Bogolyubov–de Gennes) stability analysis by identifying the relevant precession mode dependence on μ but also through direct numerical computations of the vortex evolution in the large-μ, so-called Thomas-Fermi, limit. Additionally, the dependence of the precession frequency on the distance to the trap center of an initially displaced vortex is examined, and the corresponding predictions are tested against numerical results.

DOI: 10.1103/PhysRevA.96.043612

I. INTRODUCTION

In the past two decades, the study of the dynamics of quantized vortices, few-vortex clusters, and large-scale vortex lattices has seen considerable development due to the experimental capabilities rendered available in the context of atomic Bose-Einstein condensates (BECs) [1–3]. More specifically, some of the relevant developments have encompassed (but have not been limited to) the study of the excitation and also the precession of few vortices [4–10], the observation of the instability and decay of higher charged vortices into singly charged ones [11,12], and the formation of vortices and vortex rings via the transverse instability of dark solitons [13–15]. At the level of large numbers of vortices, some of the focal points have been the internal modes (collective excitations) of vortex lattices [16–20] and the study of quantum turbulence and associated energy cascades [21–23]. In recent works, finite-temperature effects have also started to be more systematically investigated, including the formation of thermally activated vortex pairs [24] and the relevant dissipation-induced dynamics of such pairs [25]. Admittedly, it is difficult to fit all the developments (even just the experimental ones) in this partial list, yet we believe that this list provides a substantial flavor of the wide range of relevant activity.

At the same time, the last few years have seen a tremendous increase in the control over the experimental settings. On the one hand, recent techniques have made it possible to "paint" arbitrary types of potentials in atomic BECs [26]. On the other hand, there has been a significant array of developments enabling the extreme tunability of interactions in atomic gases via the utilization of mechanisms such as the Feshbach resonance [27]. The latter also continues to be a source of significant insights regarding the formation of coherent structures, their interactions, relative phases, and so on [28].

The present contribution is at the interface between the two above themes. The ability of numerous experimental groups to construct a variety of potentials, including toroidal ones (see Refs. [29,30] for some select examples), renders natural the question of the motion of the vortices and their precession frequency in more general such potentials. Our aim in the present work is to use the general methodology of Ref. [31] (see also Refs. [32,33]) in order to extract the equation of motion of vortices, in principle, in arbitrary radial potentials $V(r)$. To obtain more concrete results, we subsequently constrain the methodology a bit further to radial power potentials of the form $V(r) = k_p r^p$. For such potentials, we derive the equation of motion of a vortex, and restricting considerations to the vicinity of $r \to 0$, we infer the precession frequency in the vicinity of the trap center. It is well known that in the case of the parabolic potential, $p = 2$, this frequency has a logarithmic correction, namely, $\omega \sim \Omega^2/(2\mu)\ln(\mu/\Omega)$, where μ is the chemical potential (i.e., the background density at the trap center) and Ω sets the trap strength according to $k_2 = \frac{1}{2}\Omega^2$ (see, e.g., Ref. [33] and the more recent discussions of Refs. [34,35]). Yet, here, we find the somewhat surprising result that for general $p > 2$ and large μ, the frequency decays as $\omega \sim \mu^{-2/p}$, i.e., there is no logarithmic correction. We identify the general precession frequency and corroborate numerically both the case of $p = 2$ and those of $p = 4$ and $p = 6$. Furthermore, we explore how this precession frequency in the immediate vicinity of the origin is modified for a vortex located off center and compare these results with direct numerical simulations.

Our presentation is structured as follows. In Sec. II, we provide the theoretical formulation and the associated analytical results. In Sec. III, we compare these findings with numerical results for both the stability and the dynamics.

*wenlongcmp@gmail.com
†http://nlds.sdsu.edu

Finally, in Sec. IV we summarize our findings and present some challenges for future work.

II. MODEL AND THEORETICAL ANALYSIS

A. The Gross-Pitaevskii equation

In the framework of mean-field theory and for sufficiently low temperatures, the dynamics of a quasi-two-dimensional repulsive BEC, confined by a time-independent trap V, is described by the following dimensionless Gross-Pitaevskii equation (GPE; see Ref. [3] for relevant reductions to dimensionless units):

$$i\frac{\partial\psi}{\partial t} = -\frac{1}{2}\nabla^2\psi + V\psi + |\psi|^2\psi, \tag{1}$$

where $\psi(x,y,t)$ is the macroscopic wave function. As indicated above, the aim of our analysis is to explore a general radial potential $V(r)$, although we more specifically have in mind (considering a Taylor expansion of the general potential) a power law of the form

$$V_p(r) = k_p r^p,$$

where $r = \sqrt{x^2+y^2}$ denotes the radial variable. Some of the focal point examples in what follows (especially in our connection with numerical computations) will consist of the cases $p = 2$, 4, and 6. Note that the potential has rotational symmetry with respect to the origin, and the case of $p = 2$ corresponds to the usual harmonic trap [1,2].

In this system, we seek stationary states of the form

$$\psi(\vec{r},t) = \psi^{(0)}(\vec{r})e^{-i\mu t},$$

where μ is the chemical potential; substitution in Eq. (1) leads to the time-independent GPE:

$$-\tfrac{1}{2}\nabla^2\psi^{(0)} + V\psi^{(0)} + |\psi^{(0)}|^2\psi^{(0)} = \mu\psi^{(0)}. \tag{2}$$

We will seek such states in the form of a vortex, i.e., states bearing a radial profile with $\psi^{(0)} \to 0$ as $r \to 0$ (according to a power law $\psi^{(0)} \sim r$) and also decaying to zero due to the trap effect at large r. The phase profile involves a rotation by 2π (due to their robust stability we focus on single-charge vortices) and lends the wave function a structure $\psi \sim \exp(i\theta)$, where θ is the polar variable.

B. Theoretical analysis of precession frequencies

In the work of Ref. [31] (as well as in the earlier one of Ref. [32] and also in the review of Ref. [33]), it was realized that in describing the precessing motion of the vortex in the prototypical parabolic trap, it suffices to consider the vortex as bearing solely a phase structure without considering in detail its density profile. However, it should be mentioned in passing here that the latter is also possible (yet it leads to rather comparable results), as developed using a hyperbolic tangent approximation of the density [36]. In that light, we will utilize the relevant simplified ansatz for a singly charged (point) vortex located at position (x_1,y_1),

$$\psi = \psi_{\rm TF}\exp(iS), \quad S = \tan^{-1}\left(\frac{y-y_1}{x-x_1}\right), \tag{3}$$

where $\psi_{\rm TF} = \sqrt{\max(\mu - V,0)}$ is the Thomas-Fermi (TF) ground state. By means of this variational approximation for the wave function, it is possible to identify the kinetic energy of the vortex field as [32]

$$T = \frac{i}{2}\int_{\mathbb{R}^2}(\psi^*\psi_t - \psi_t^*\psi)\,dx\,dy$$
$$\approx -2\pi\dot{\phi}_1\int_0^{r_1}[\mu - V(a)]a\,da,$$

where $r_1 = \sqrt{x_1^2+y_1^2}$ is the distance of the vortex to the center of the trap and ϕ_1 is the polar angle for the vortex position (an asterisk denotes the complex conjugate, and an overdot denotes differentiation with respect to t). Using the ansatz (3), it is also possible to express the (potential) energy of the system:

$$E = \int_{\mathbb{R}^2}\left[\frac{1}{2}|\nabla\psi|^2 + V|\psi|^2 + \frac{1}{2}|\psi|^4\right]dx\,dy$$
$$\approx \pi\left[\int_0^{r_1-\xi} r\,\frac{\mu - V(r)}{r_1^2 - r^2}dr + \int_{r_1+\xi}^{R_{\rm TF}} r\,\frac{\mu - V(r)}{r^2 - r_1^2}dr\right], \tag{4}$$

where $\xi = 1/\sqrt{2\mu}$ is vortex core width (given by the healing length) and $R_{\rm TF}$ is the TF radius such that $V(R_{\rm TF}) = \mu$. As proposed in Ref. [31], the above result is based on the regularization of the energy integral by removing a "layer" of width 2ξ about the singularity at r_1. In the present work we extend this methodology to general radially symmetric potentials. Details of the relevant derivation are provided in Appendix A.

Considering now the Lagrangian $L = T - E$, one can obtain the resulting dynamical equation of motion for the vortex precession. In this case, the obtained evolution is along the azimuthal direction and of the form [32]

$$\dot{\phi}_1 = \frac{-1}{2\pi r_1[\mu - V(r_1)]}\frac{\partial E}{\partial r_1}. \tag{5}$$

While it is clear that the radial potential will generically result in precessional dynamics, it is instructive to consider some special-case examples (including the well-known, experimentally relevant one of the parabolic trap as a benchmark).

C. Parabolic trap $V(r) = \frac{1}{2}\Omega^2 r^2$

For a parabolic trap $V(r) = \frac{1}{2}\Omega^2 r^2$, the energy reads

$$E = \frac{\pi\Omega^2}{4}\left[2\left(\xi^2 + r_1^2\right) - R_{\rm TF}^2 + \left(r_1^2 - R_{\rm TF}^2\right)\ln\left(\frac{\xi^2\left(4r_1^2 - \xi^2\right)}{r_1^2\left(R_{\rm TF}^2 - r_1^2\right)}\right)\right],$$

where $R_{\rm TF}^2 = 2\mu/\Omega^2$. The above expression for the energy leads, via Eq. (5), to the following equation of motion:

$$\dot{\phi}_1 = \frac{4r_1^2 - \xi^2 R_{\rm TF}^2 - r_1^2\left(\xi^2 - 4r_1^2\right)\ln\frac{\xi^2\left(4r_1^2-\xi^2\right)}{r_1^2\left(R_{\rm TF}^2-r_1^2\right)}}{2r_1^2\left(\xi^2 - 4r_1^2\right)\left(R_{\rm TF}^2 - r_1^2\right)}.$$

If we now consider the motion near the center, taking a large chemical potential so that $1/\sqrt{2\mu} \equiv \xi \to 0$ but also

$r_1 \to 0$ (with $r_1 \gg \xi$), we retrieve the well-known result [33] according to which the precession frequency is approximated as

$$\omega = \frac{\Omega^2}{2\mu} \ln\left(\frac{\mu}{\Omega}\right). \tag{6}$$

Notice that subsequent works (see, e.g., Ref. [34]) devised numerically inspired corrections to this formula, although not to its functional form, yet it has been particularly successful in capturing the functional form of the dependence on the chemical potential μ (and the frequency Ω).

D. The quartic potential $V(r) = k_4 r^4$

For a quartic potential, $V(r) = k_4 r^4$, the TF radius is given by $k_4 R_{\rm TF}^4 = \mu$. In this case, the potential energy can still be calculated analytically:

$$E = \frac{\pi k_4}{4}\Bigg[2\xi^4 + 16\xi^2 r_1^2 + 6r_1^4 - 2r_1^2 R_{\rm TF}^2 - R_{\rm TF}^4 + 2\left(r_1^4 - R_{\rm TF}^4\right)\ln\left(\frac{\xi^2\left(4r_1^2 - \xi^2\right)}{r_1^2\left(R_{\rm TF}^2 - r_1^2\right)}\right)\Bigg].$$

Naturally, the dynamics can be extracted from Eq. (5), yet it is too unwieldy and not particularly informative to provide here. Instead, we focus once again on the limit of $\xi, r_1 \to 0$, with ξ tending faster to the limit. The remarkable observation here, and in general for other powers $p > 2$ that we have examined, is that the logarithmic term tends to zero (due to its proportionality to some power of r_1). Hence, the logarithmic correction *does not survive* as it does in the parabolic case. Instead, in this case, the limit reads

$$\dot{\phi}_1 = \omega = \frac{1}{R_{\rm TF}^2} \sim \mu^{-\frac{1}{2}}. \tag{7}$$

E. General power $V(r) = k_p r^p$

For a radially symmetric potential $V(r) = k_p r^p$ with general power p, we have $\mu = k_p R_{\rm TF}^p$. Remarkably, the general form of the energy is again available in analytic form for arbitrary p:

$$E = \frac{\pi k_p}{2}\Bigg\{r_1^p\left[B\left(\frac{r_1^2}{R_{\rm TF}^2}, -\frac{p}{2}, 0\right) - B\left(\frac{r_1^2}{(\xi + r_1)^2}, -\frac{p}{2}, 0\right)\right] - 2(r_1 - \xi)^{2+p}\,{}_2F_1\left[1, \frac{p+2}{2}, \frac{p+4}{2}, \left(\frac{r_1 - \xi}{r_1}\right)^2\right] - R_{\rm TF}^p \ln\left(\frac{\xi^2\left(4r_1^2 - \xi^2\right)}{r_1^2\left(R_{\rm TF}^2 - r_1^2\right)}\right)\Bigg\}, \tag{8}$$

where B denotes the incomplete beta function and F denotes the hypergeometric function. By considering integer p, the resulting asymptotics in the limit of $\xi \to 0$ and $r_1 \to 0$ (with $r_1 \gg \xi$) from the gradient of E [in Eq. (8)] leads to

$$\dot{\phi}_1 = \omega = \frac{p}{2(p-2)}\frac{1}{R_{\rm TF}^2} \sim \mu^{-\frac{2}{p}}, \tag{9}$$

which is consistent with the $p = 4$ result of Eq. (7). In the general asymptotic form of Eq. (8), the corresponding prefactor $\frac{p}{2(p-2)}$ is evidently different for different values of p, but importantly, the scaling relation is general, providing an explicit power-law prediction for the dependence of the precession frequency on the chemical potential [i.e., the background density, which also controls the healing length (width) scale of the vortex].

It is important to stress that the logarithmic term in the energy, and hence in the precession frequency, is always present independent of the chosen power p of the confining potential. This logarithmic term is crucial (dominant) for parabolic trapping potentials [see Eq. (6) and Refs. [33,37]]. However, as shown above, for potentials with powers larger than quadratic, the logarithmic term decays faster than the remaining terms in the asymptotic expression near the origin, and hence, it is no longer dominating the relevant asymptotics. Nonetheless, it should be pointed out that far from the origin, the logarithmic correction terms will indeed become significant, and the full expression without discarding these terms needs to be used.

In order to complement the above result for the precession frequency using the asymptotics for the energy, we have also employed a direct matching asymptotic analysis on Eq. (1) that yields precisely the same asymptotic result as in Eq. (9). Details on this matched asymptotic procedure can be found in Appendix B. We now turn to a numerical examination of the relevant findings.

III. NUMERICAL RESULTS

In our numerical work, we study $V = \frac{1}{p}r^p$, where $p = 2,4$, and 6. We start by showing the ground and vortex states at a typical (relatively large) value of the chemical potential, $\mu = 40$, within the so-called Thomas-Fermi regime. In this regime, the radial background density (i.e., the density of the ground state) can be well approximated as $|\psi|^2 \approx |\psi_{\rm TF}|^2 = \mu - V(r)$. Relevant results as depicted in Fig. 1. One can observe that the states near $r = 0$ are almost identical for different potentials. In particular, the density of the ground states at $r = 0$ and the width of the vortices is essentially dominated by the chemical potential, which controls the corresponding healing length. The size of the states gets smaller as p increases or, equivalently, as the atoms are bound tighter.

Let us start by showing the numerical results for the parabolic potential $V(r) = \frac{1}{2}r^2$ (i.e., $\Omega = 1$). The Bogolyubov–de Gennes (BdG) stability spectrum for the steady state consisting of a unit-charge vortex at the center of the trap is depicted in Fig. 2. Among all the modes in the spectrum, the lowest is the one that is *not* found in the spectrum of linearization around the ground state. Instead, when we excite this mode, we find that it leads the vortex to a precessional motion around the center of the trap; thus, the frequency of this mode corresponds to the frequency of the associated precession [34]. This precessional mode is depicted with an orange line in Fig. 2.

We now go beyond the well-known parabolic case in order to examine other examples that the general theory can tackle. More specifically, we consider the quartic case of $p = 4$ and the sextic case of $p = 6$. The BdG spectra for the corresponding steady-state vortex configurations are shown in Fig. 3. Note that both potentials still have the vortex precession

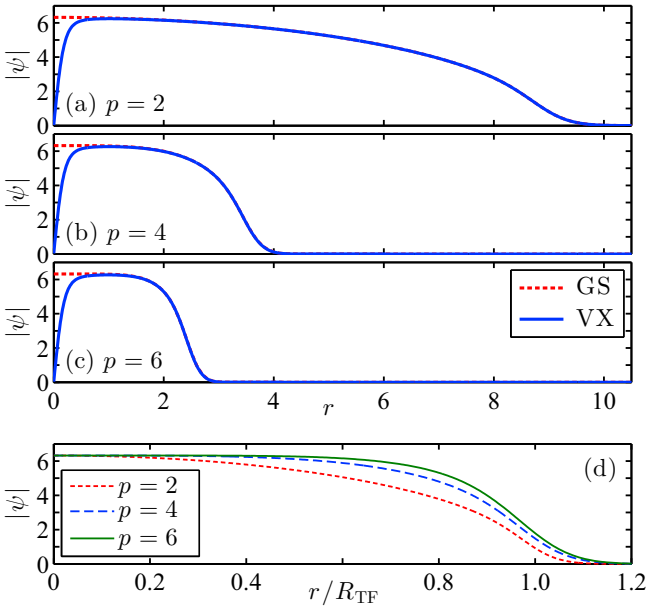

FIG. 1. Radial profile $|\psi|$ as a function of r for the ground state (GS, red dashed line) and the vortex state (VX, blue solid line) inside the trapping potential $V(r) = \frac{1}{p}r^p$ with $\mu = 40$ for (a) $p = 2$, (b) $p = 4$, and (c) $p = 6$. Note that in the Thomas-Fermi limit, the size of the vortices for the different potentials is essentially the same. This property, determined by the healing length, is controlled by the chemical potential μ, which is constant ($\mu = 40$) for the three cases. (d) GS profiles as a function of the rescaled distance $r/R_{\rm TF}$, where the corresponding TF radii are given by $R_{\rm TF} = (p\mu)^{1/p}$.

mode (see eigenfrequency mode depicted in orange) because of the symmetry of the potential. Indeed, we find that in both cases it remains the only mode asymptoting to $\omega = 0$, as the chemical potential μ is increased. The examples of the associated dynamics that we have chosen to show are for $\mu = 40$. This is much larger than that of the case $p = 2$ because the cases $p = 4$ and $p = 6$ involve a tighter-binding

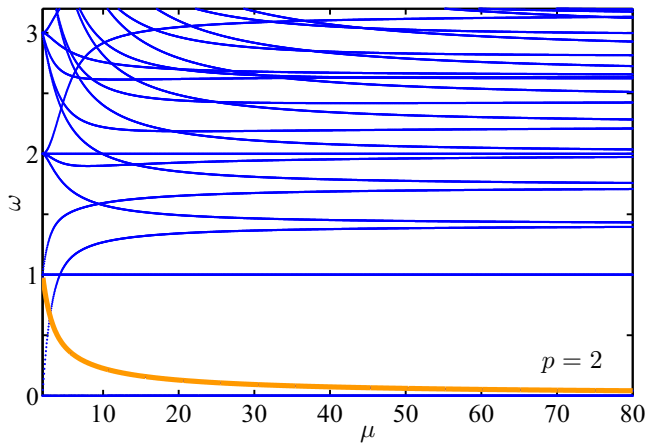

FIG. 2. The BdG spectrum for the vortex in the quadratic potential. The lowest mode, highlighted in orange, is the one of interest as it corresponds to the vortex precession around the trap center.

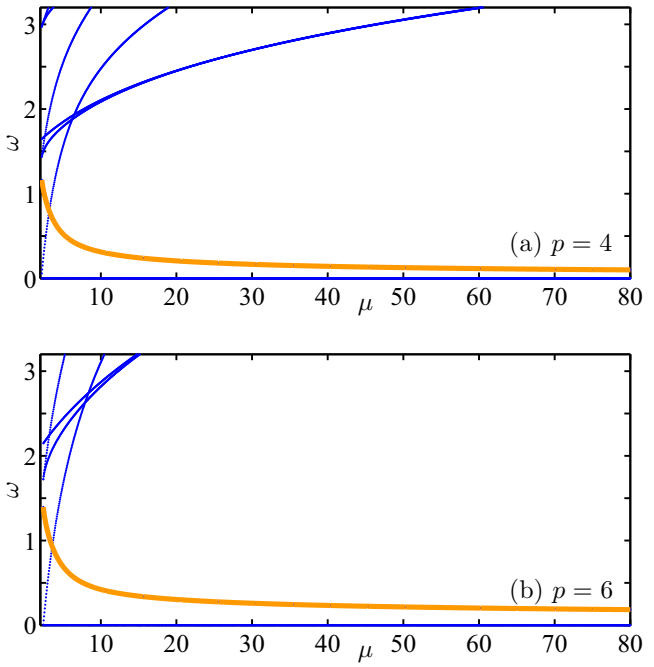

FIG. 3. The vortex spectrum in the (a) quartic and (b) sextic potentials. The lowest mode, which is highlighted in orange similar to the quadratic potential, is the vortex precession mode around the trap center.

trap. It is interesting to note that the vortex in all three cases is remarkably stable for all the values of the chemical potential that we have examined.

Let us now focus on the scaling of the precession frequency ω (close to the center of the trap) on the chemical potential for all three cases of $p = 2$, 4, and 6. The corresponding results are depicted in Fig. 4 and are compared to our theoretical prediction, as encapsulated in Eq. (9).[1] In Fig. 4, the relevance of our analytical prediction, especially of the corresponding scaling, is evident. Indeed, once the (small- and) intermediate-chemical-potential regime (where all potentials scale similarly) is bypassed and the large-chemical-potential TF regime is reached, the different potentials scale differently. More specifically, it is found that the scaling prediction of Eq. (9) is closely followed by the spectral numerical results for $p = 4$ and $p = 6$ (see the thin solid blue and green lines, respectively). On the other hand, for $p = 2$, the prediction of Eq. (9) (see the red dashed line) is incorrect as the dominant term in this case has a logarithmic form [see Eq. (6) and the thin solid red line in Fig. 4]. It is worth mentioning that, although the precession frequency predicted by Eq. (6) has the correct scaling, a numerical factor has been used in order

[1]It is worth mentioning that a key feature of our numerical results for the computation of the BdG spectra is that we use numerical methods that we have described in earlier works [38], involving a quasi-one-dimensional radial computation (for different azimuthal wave numbers). This allows us to explore large values of the chemical potential to reach the TF limit, where our analytical prediction is relevant (since there the internal density structure of the vortex can be ignored).

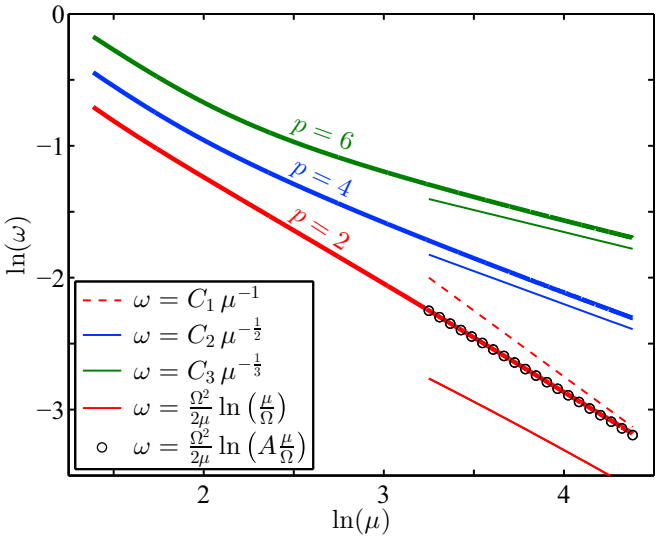

FIG. 4. Scaling of the precession frequency ω on the chemical potential μ. The thick lines correspond to the precession frequency extracted from the numerically obtained spectra, and the asymptotic approximations are depicted with thin lines (C_i are arbitrary constants chosen for ease of exposition). The case of $p = 2$ decays slower than the power scaling (see thin red dashed line) due to the logarithmic correction, while for $p = 4$ and $p = 6$, the predictions and the spectrum appear to compare well with each other, suggesting good agreement with the analytical prediction of Eq. (9). The black circles correspond to a correction to the asymptotic formula (6), namely, Eq. (10) with $A = 8.88$ (see Ref. [34]).

to incorporate the subdominant contributions to the frequency scaling according to μ^{-1} [34] in a quantitative fashion. This is depicted by the black circles Fig. 4 corresponding to

$$\omega = \frac{\Omega^2}{2\mu} \ln\left(A\frac{\mu}{\Omega}\right), \tag{10}$$

with the numerical factor $A = 8.88$ (see Ref. [34]).

To complement the description for the vortex precession around the center of the trap, we also measure the dependence of this frequency as the vortex is shifted away from $r = 0$. In practice, a straightforward way to observe this precession involves shifting the vortex off of its equilibrium position at $r = 0$ and then following its circular motion around the center.[2] Figure 5 depicts the departure of the precession frequency from the corresponding eigenfrequency ω_0 at $r = 0$ measured from the center of the trap. Figure 5 also depicts the analytical prediction found from evaluating Eq. (5) and using the limit $\xi \ll r$ (see solid curves). It is evident from these results that the theory underestimates the precession frequency. We attribute this discrepancy to two possible factors:

(a) The ansatz used in the theory completely disregards the internal spatial structure of the vortex as it effectively treats it as a point vortex, an approximation valid as $\mu \to \infty$. For instance, optimizing the vortex width appears to be an important factor in the success of more refined (yet less straightforwardly tractable in the general case) variational approaches such as that of Ref. [36].

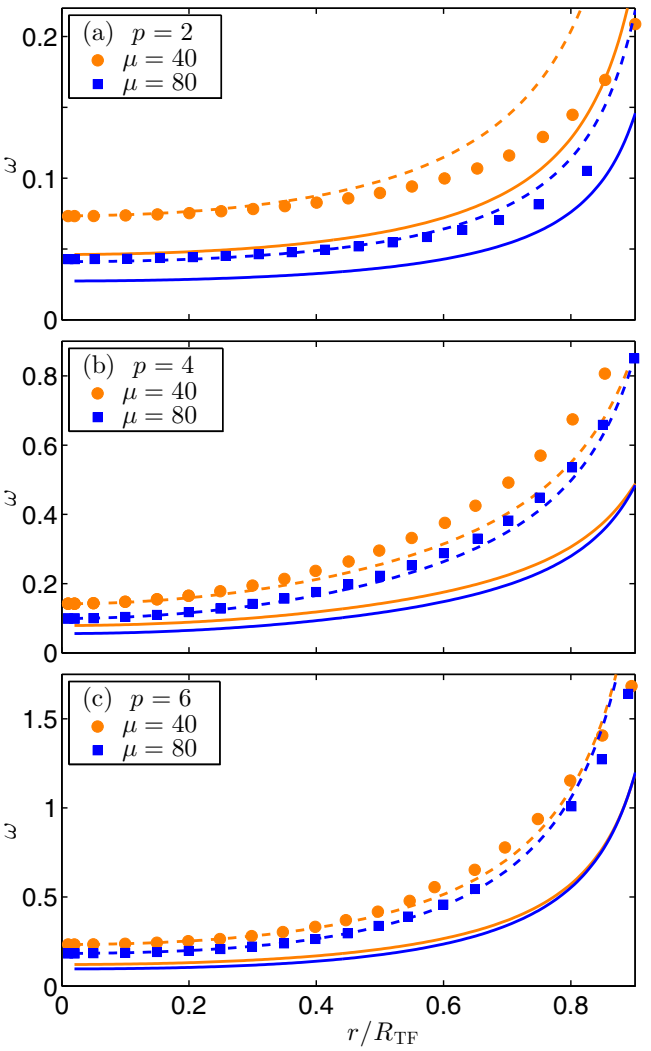

FIG. 5. Scaling of the precession frequency as a function of the rescaled vortex position for the different potentials $V(r) = \frac{1}{p}r^p$ with $\mu = 40$ and $\mu = 80$. A vortex is displaced from $r = 0$, and its precession frequency is extracted from its dynamical evolution (see text) and depicted with orange (blue) circles (squares) for $\mu = 40$ ($\mu = 80$). The solid lines depict the theoretical predictions from evaluating Eq. (5) and using the limit $\xi \ll r$. The dashed curves for the $p = 2$ case correspond to the corrected precession of Eq. (10), while the dashed curves for the $p = 4$ and $p = 6$ cases depict the rescaled theoretical predictions to match the precession frequency in the limit $r = 0$. These rescaling coefficients correspond to, for $\mu = 40$ and $\mu = 80$, respectively, 1.7944 and 1.7804 for $p = 4$ and 1.9302 and 1.9114 for $p = 6$.

[2]We should mention that the actual vortex orbit is not exactly circular as the vortex pushes a small amount mass out away from its core, and as it precesses, dipolar and quadrupolar modes of the background cloud are weakly excited. Nevertheless, it is possible to accurately measure the oscillation frequency by following the dynamics for a sufficiently long time; here, we typically integrate all dynamics up to $t = 1000$ and apply a least-squares fit using a sine function. We identify the location of the vortex during the dynamics by looking for the density minimum in the neighborhood of the vortex using a finer-grid cubic spline interpolation.

(b) Second, when estimating the precession frequency at the center of the trap ($r = 0$) the limit $0 < \xi \ll r$ is obviously violated as the healing length ξ is finite.

Although the theoretical results fail to precisely predict the precession frequency at $r = 0$, they are able to give the right tendency for the departure of the precession frequency as the vortex is displaced away from the origin. In fact, after applying suitable modifications (see dashed curves in Fig. 5), the predictions produce a good quantitative match for the departure of the precession frequency from ω_0 as r departs from $r = 0$ (especially for small and intermediate values of r; the match is progressively better for larger values of μ, in line with the underlying premise of the theory). Specifically, in the $p = 2$ case, where the dominant term on the precession as a function of r is logarithmic, we employ the correction given in Eq. (10) [34]. On the other hand, for the $p = 4$ and $p = 6$ cases, the dominant terms are algebraic, and thus, we opt for a multiplicative rescaling factor chosen to match the precession frequency at the origin (see Fig. 5).

IV. CONCLUSIONS AND FUTURE CHALLENGES

In the present work, we have explored the motion of vortices in general radially symmetric potentials. We have found that similar to the well-known parabolic case, the motion of the vortices involves a precession. The main result of the present work concerns the vortex precession frequency and its dependence on both the chemical potential of the background cloud and the location of the vortex within the condensate. Utilizing a variational formulation generalizing the work of Ref. [33], we were able to provide closed-form expressions for the precession frequency relevant in the large-chemical-potential limit (Thomas-Fermi regime). These expressions permitted us to appreciate the power-law scaling of the precession frequency on the chemical potential and how the relevant dependence becomes slower as p increases. The limitations of the theory in identifying the precession mode frequency at the origin were explained, and it was shown how a suitable amendment can be used to capture the frequency dependence on the radial position of an off-center vortex.

While in the present work we have explored the general (radial) potential motion of a single vortex, numerous related questions naturally emerge from this study. Here, we considered isotropic potentials which still constitute a subject of active investigation [39] and some controversy regarding the physical interpretation of the origin of the vortex motion [40]. Yet anisotropic potentials are also quite relevant in atomic BECs [3,33]. Examining vortex motion in such anisotropic settings under general V would certainly be of interest. Furthermore, combining an understanding of the single-vortex motion in a general potential with that of the intervortex interaction will enable identifying multivortex (cluster and crystal) states for arbitrary trapped BEC systems. Another possibility for future research could be to consider pseudopotentials stemming from considering space- (radially-) dependent nonlinearities [41] with different power-law prescriptions.

Finally, while it is natural to develop the above ideas first in two-dimensional settings, generalizing them to vortex rings in three-dimensional frameworks [42] would also be of interest in its own right. Some of these directions are currently under consideration and will be reported in future publications.

ACKNOWLEDGMENTS

We thank A. Esposito, R. Krichevsky, and A. Nicolis for bringing up their related work on vortex precession in trapped superfluids from effective-field theory [39] and for subsequent stimulating discussions. W.W. acknowledges support from Grant No. NSF-DMR-1151387. P.G.K. gratefully acknowledges the support of Grants No. NSF-DMS-1312856 and No. NSF-PHY-1602994, as well as from the ERC under FP7, Marie Curie Actions, People, International Research Staff Exchange Scheme (IRSES-605096) and the Greek Diaspora Fellowship Program. P.G.K. also acknowledges useful discussions with Prof. T. Kolokolnikov. R.C.-G. acknowledges support from Grants No. NSF-DMS-1309035 and No. PHY-1603058. The work of W.W. is supported in part by the Office of the Director of National Intelligence (ODNI), Intelligence Advanced Research Projects Activity (IARPA), via MIT Lincoln Laboratory Air Force Contract No. FA8721-05-C-0002. The views and conclusions contained herein are those of the authors and should not be interpreted as necessarily representing the official policies or endorsements, either expressed or implied, of ODNI, IARPA, or the U.S. Government. The U.S. Government is authorized to reproduce and distribute reprints for Governmental purpose notwithstanding any copyright annotation thereon. We thank Texas A&M University for access to their Ada and Curie clusters.

APPENDIX A: ENERGY CALCULATION

As explained in Ref. [31], the principal contribution to the energy stems from the gradient term, which upon our ansatz (3) and in the TF approximation can be written as

$$E = \frac{\mu}{2}\int_0^{R_{\rm TF}} r dr \int_0^{2\pi} d\theta \left(1 - \frac{V(r)}{\mu}\right) \times \frac{1}{r^2 + r_1^2 - 2rr_1\cos(\theta - \phi_1)},$$

where, again, $(r1,\phi_1)$ is the vortex position in polar coordinates. This integral can be split into two radial contributions, namely, the integral I_1 from zero to $r_1 - \xi$ and I_2 from $r_1 + \xi$ to $R_{\rm TF}$. In this way, using the characteristic length of the vortex core, namely, the healing length ξ, we regularize the integral. These two integrals can then be rewritten as

$$I_1 = \frac{1}{2}\int_0^{r_1-\xi} dr \int_0^{2\pi} d\theta \, \frac{r[\mu - V(r)]}{r_1^2 - r^2} \times \left\{1 + 2\sum_n \left(\frac{r}{r_1}\right)^n \cos[n(\theta - \phi_1)]\right\},$$

$$I_2 = \frac{1}{2}\int_{r_1+\xi}^{R_{\rm TF}} dr \int_0^{2\pi} d\theta \, \frac{r[\mu - V(r)]}{r^2 - r_1^2} \times \left\{1 + 2\sum_n \left(\frac{r_1}{r}\right)^n \cos[n(\theta - \phi_1)]\right\},$$

which finally yield the following resulting expressions used in Eq. (4):

$$I_1 = \pi \int_0^{r_1-\xi} dr \frac{r[\mu - V(r)]}{r_1^2 - r^2},$$

$$I_2 = \pi \int_{r_1+\xi}^{R_{\rm TF}} dr \frac{r[\mu - V(r)]}{r^2 - r_1^2}.$$

APPENDIX B: MATCHED ASYMPTOTICS CALCULATION

We hereby obtain an alternative derivation for the precession frequency of Eq. (9) using matched asymptotics directly in the original model (1). We seek stationary solutions to Eq. (1) of the form $\psi = \psi^{(0)} e^{-i\mu t}$ satisfying the steady-state equation (2). By scaling variables using $\tilde{x} = x/R_{\rm TF}$, $\tilde{y} = y/R_{\rm TF}$, $\tilde{\psi} = \psi^{(0)}/\sqrt{\mu}$, and $\tilde{t} = t/(2R_{\rm TF}^2)$, we obtain

$$-i\psi_t = \Delta\psi + \frac{1}{\varepsilon^2}[1 - V(r) - |\psi|^2]\psi,$$

with $\varepsilon^2 = 1/(2R_{\rm TF}^2\mu)$ and where, for ease of exposition, we have dropped tildes and superscripts. Note that the core size of the vortex is of order ε.

Away from the core of the vortex, to leading order in ε, we have $1 - V(\vec{r}) - |\psi(\vec{r})|^2 = 0$, which suggests the separation

$$\psi = \psi_{\rm TF}\, e^{iS},$$

where $\psi_{\rm TF} = \sqrt{1 - V(\vec{r})}$ is the TF approximation and S satisfies

$$\psi_{\rm TF}\Delta S + 2\nabla\psi_{\rm TF}\cdot\nabla S = 0,$$
$$\nabla\times\nabla S = 2\pi\delta(\vec{r} - \vec{r}_1),$$

where δ is the Dirac delta function centered at the vortex location $\vec{r}_1$. By examining the local behavior of S, we can obtain

$$\psi(\vec{r}) \sim [\psi_{\rm TF}(\vec{r}_1) + \nabla\psi_{\rm TF}(\vec{r}_1)\cdot(r - \vec{r}_1)]e^{i\varphi}\left(1 + i\ln|\vec{r} - \vec{r}_1|\frac{\nabla^\perp\psi_{\rm TF}(\vec{r}_1)}{\psi_{\rm TF}(\vec{r}_1)}\cdot(\vec{r} - \vec{r}_1) + \vec{K}\cdot(\vec{r} - \vec{r}_1)\right), \text{ as } \vec{r}\to\vec{r}_1, \tag{B1}$$

where $\vec{K} \equiv \lim_{\vec{r}\to\vec{r}_1}\nabla(S - \varphi)$, $\varphi = \text{ang}(\vec{r} - \vec{r}_1)$, and the operator $(\cdot)^\perp$ is defined, in Cartesian coordinates, by $(a,b)^\perp \equiv (-b,a)$. Near the core of the vortex, we denote the stretched variable $\vec{\rho} = [\vec{r} - \vec{r}_1(t)]/\varepsilon$ and look for the solution in the form

$$\psi = \psi_0(\vec{\rho}) + \varepsilon\psi_1(\vec{\rho}) + \cdots.$$

Matching the first two orders of ε yields

$$0 = \Delta_{\vec{\rho}}\psi_0 + [1 - V(|\vec{r}_1|)]\psi_0 - |\psi_0|^2\psi_0,$$

$$i\,\dot{\vec{r}}_1\cdot\nabla_{\vec{\rho}}\psi_0 + \nabla V(\vec{r}_1)\cdot\vec{\rho}\,\psi_0 = \Delta_{\vec{\rho}}\psi_1 + [1 - V(|\vec{r}_1|)]\psi_1 - |\psi_0|^2\psi_1 - \psi_0\left(\psi_0\psi_1^* + \psi_1\psi_0^*\right),$$

where the overdot denotes the time derivative. Now, in order to match the outer region, we need only the asymptotic behavior of the inner solution as $|\vec{\rho}|\to\infty$. A detailed analysis for this asymptotics yields [43]

$$\psi_0 \to \psi_{\rm TF}e^{i\theta}, \qquad \text{as } |\vec{\rho}|\to\infty,$$

$$\psi_1 \to \left(\nabla\psi_{\rm TF}(\vec{r}_1)\cdot\vec{\rho} + i\ln(\psi_{\rm TF}|\vec{\rho}|)\nabla^\perp\psi_{\rm TF}\cdot\vec{\rho} + \frac{1}{2}\psi_{\rm TF}(\vec{r}_1)\dot{\vec{r}}_1\cdot\vec{\rho}\right)e^{i\theta}, \qquad \text{as } |\vec{\rho}|\to\infty,$$

and therefore,

$$\psi = \psi_{\rm TF}(\vec{r}_1)e^{i\theta} + \varepsilon\left(\nabla\psi_{\rm TF}(\vec{r}_1)\cdot\vec{\rho} + i\ln(\psi_{\rm TF}|\vec{\rho}|)\nabla^\perp\psi_{\rm TF}(\vec{r}_1)\cdot\vec{\rho} + \frac{1}{2}\psi_{\rm TF}(\vec{r}_1)\dot{\vec{r}}_1\cdot\vec{\rho}\right)e^{i\theta}, \text{ as } |\vec{\rho}|\to\infty. \tag{B2}$$

Employing asymptotic matching between Eqs. (B1) and (B2), recalling that $\vec{\rho} = [\vec{r} - \vec{r}_1(t)]/\varepsilon$, yields

$$\frac{-2\vec{K} + \dot{\vec{r}}_1}{\ln\varepsilon - \ln[\psi_{\rm TF}(\vec{r}_1)]} - \frac{2\nabla^\perp\psi_{\rm TF}(\vec{r}_1)}{\psi_{\rm TF}(\vec{r}_1)} = 0.$$

Thus, to leading order of $\nu \equiv -1/\ln\varepsilon$, we obtain

$$\dot{\vec{r}}_1 = -\frac{2}{\nu}\frac{\nabla^\perp\psi_{\rm TF}(\vec{r}_1)}{\psi_{\rm TF}(\vec{r}_1)} + 2\vec{K}. \tag{B3}$$

Now, depending on the range of $|\vec{r}_1|$, we have two different leading-order dynamics:
(a) If $|\nabla^\perp\psi_{\rm TF}(\vec{r}_1)| \ll \nu$, the dominant term in (B3) is $\vec{K}$, and thus,

$$\dot{\vec{r}}_1 = 2\vec{K}. \tag{B4}$$

(b) If $|\nabla^\perp\psi_{\rm TF}(\vec{r}_1)| \gg \nu$, the dominant term in (B3) is the first term, and thus,

$$\dot{\vec{r}}_1 = -\frac{2}{\nu}\frac{\nabla^\perp\psi_{\rm TF}(\vec{r}_1)}{\psi_{\rm TF}(\vec{r}_1)}. \tag{B5}$$

While the comparison of the relevant cases in terms of the dominant mathematical contribution is straightforward, assigning an intuitive explanation to these different scenarios is an open topic worthwhile of further consideration in future studies. By returning to the original (unscaled) variable t, Eq. (B4) finally yields the following expression for the rate of change of the vortex position vector $\vec{r}_1$:

$$\dot{\vec{r}}_1 = \frac{\vec{K}}{R_{\rm TF}^2},$$

which, by noting that $\vec{K}$ is an azimuthal vector, is in agreement with the precession frequency that was obtained using the asymptotic expansion for the energy in Sec. II E:

$$\omega \sim \frac{1}{R_{\rm TF}^2}. \tag{B6}$$

[1] C. J. Pethick and H. Smith, *Bose-Einstein Condensation in Dilute Gases* (Cambridge University Press, Cambridge, 2002).

[2] L. P. Pitaevskii and S. Stringari, *Bose-Einstein Condensation* (Oxford University Press, Oxford, 2003).

[3] P. G. Kevrekidis, D. J. Frantzeskakis, and R. Carretero-González, *The Defocusing Nonlinear Schrödinger Equation* (Society for Industrial and Applied Mathematics, Philadelphia, 2015).

[4] B. P. Anderson, P. C. Haljan, C. E. Wieman, and E. A. Cornell, Phys. Rev. Lett. **85**, 2857 (2000).

[5] P. C. Haljan, B. P. Anderson, I. Coddington, and E. A. Cornell, Phys. Rev. Lett. **86**, 2922 (2001).

[6] V. Bretin, P. Rosenbusch, F. Chevy, G. V. Shlyapnikov, and J. Dalibard, Phys. Rev. Lett. **90**, 100403 (2003).

[7] T. W. Neely, E. C. Samson, A. S. Bradley, M. J. Davis, and B. P. Anderson, Phys. Rev. Lett. **104**, 160401 (2010).

[8] D. V. Freilich, D. M. Bianchi, A. M. Kaufman, T. K. Langin, and D. S. Hall, Science **329**, 1182 (2010).

[9] S. Middelkamp, P. J. Torres, P. G. Kevrekidis, D. J. Frantzeskakis, R. Carretero-González, P. Schmelcher, D. V. Freilich, and D. S. Hall, Phys. Rev. A **84**, 011605(R) (2011).

[10] R. Navarro, R. Carretero-González, P. J. Torres, P. G. Kevrekidis, D. J. Frantzeskakis, M. W. Ray, E. Altuntaş, and D. S. Hall, Phys. Rev. Lett. **110**, 225301 (2013).

[11] Y. Shin, M. Saba, M. Vengalattore, T. A. Pasquini, C. Sanner, A. E. Leanhardt, M. Prentiss, D. E. Pritchard, and W. Ketterle, Phys. Rev. Lett. **93**, 160406 (2004).

[12] T. Isoshima, M. Okano, H. Yasuda, K. Kasa, J. A. M. Huhtamäki, M. Kumakura, and Y. Takahashi, Phys. Rev. Lett. **99**, 200403 (2007).

[13] B. P. Anderson, P. C. Haljan, C. A. Regal, D. L. Feder, L. A. Collins, C. W. Clark, and E. A. Cornell, Phys. Rev. Lett. **86**, 2926 (2001).

[14] Z. Dutton, M. Budde, C. Slowe, and L. V. Hau, Science **293**, 663 (2001).

[15] M. J. H. Ku, B. Mukherjee, T. Yefsah, and M. W. Zwierlein, Phys. Rev. Lett. **116**, 045304 (2016).

[16] P. Engels, I. Coddington, P. C. Haljan, and E. A. Cornell, Phys. Rev. Lett. **89**, 100403 (2002).

[17] I. Coddington, P. Engels, V. Schweikhard, and E. A. Cornell, Phys. Rev. Lett. **91**, 100402 (2003).

[18] N. L. Smith, W. H. Heathcote, J. M. Krueger, and C. J. Foot, Phys. Rev. Lett. **93**, 080406 (2004).

[19] V. Schweikhard, I. Coddington, P. Engels, S. Tung, and E. A. Cornell, Phys. Rev. Lett. **93**, 210403 (2004).

[20] S. Tung, V. Schweikhard, and E. A. Cornell, Phys. Rev. Lett. **97**, 240402 (2006).

[21] E. A. L. Henn, J. A. Seman, G. Roati, K. M. F. Magalhães, and V. S. Bagnato, Phys. Rev. Lett. **103**, 045301 (2009).

[22] T. W. Neely, A. S. Bradley, E. C. Samson, S. J. Rooney, E. M. Wright, K. J. H. Law, R. Carretero-González, P. G. Kevrekidis, M. J. Davis, and B. P. Anderson, Phys. Rev. Lett. **111**, 235301 (2013).

[23] W. J. Kwon, G. Moon, J.-Y. Choi, S. W. Seo, and Y.-I. Shin, Phys. Rev. A **90**, 063627 (2014).

[24] J.-Y. Choi, S. W. Seo, and Y.-I. Shin, Phys. Rev. Lett. **110**, 175302 (2013).

[25] G. Moon, W. J. Kwon, H. Lee, and Y.-I. Shin, Phys. Rev. A **92**, 051601(R) (2015).

[26] K. Henderson, C. Ryu, C. MacCormick, and M. G. Boshier, New J. Phys. **11**, 043030 (2009).

[27] S. E. Pollack, D. Dries, M. Junker, Y. P. Chen, T. A. Corcovilos, and R. G. Hulet, Phys. Rev. Lett. **102**, 090402 (2009).

[28] J. H. V. Nguyen, D. Luo, and R. G. Hulet, Science **356**, 422 (2017); P. J. Everitt *et al.*, Phys. Rev. A **96**, 041601(R) (2017).

[29] A. Ramanathan, K. C. Wright, S. R. Muniz, M. Zelan, W. T. Hill, C. J. Lobb, K. Helmerson, W. D. Phillips, and G. K. Campbell, Phys. Rev. Lett. **106**, 130401 (2011); K. C. Wright, R. B. Blakestad, C. J. Lobb, W. D. Phillips, and G. K. Campbell, *ibid.* **110**, 025302 (2013).

[30] C. Ryu, K. C. Henderson, and M. G. Boshier, New J. Phys. **16**, 013046 (2014).

[31] J. K. Kim and A. L. Fetter, Phys. Rev. A **70**, 043624 (2004).

[32] E. Lundh and P. Ao, Phys. Rev. A **61**, 063612 (2000).

[33] A. L. Fetter and A. A. Svidzinsky, J. Phys. Condens. Matter **13**, R135 (2001).

[34] S. Middelkamp, P. G. Kevrekidis, D. J. Frantzeskakis, R. Carretero-González, and P. Schmelcher, Phys. Rev. A **82**, 013646 (2010).

[35] D. E. Pelinovsky and P. G. Kevrekidis, Nonlinearity **24**, 1271 (2011).

[36] Y. Castin and R. Dum, Eur. Phys. J. D **7**, 399 (1999).

[37] A. L. Fetter, Rev. Mod. Phys. **81**, 647 (2009).
[38] W. Wang, P. G. Kevrekidis, R. Carretero-González, and D. J. Frantzeskakis, Phys. Rev. A **93**, 023630 (2016); W. Wang and P. G. Kevrekidis, Phys. Rev. E **95**, 032201 (2017).
[39] A. Esposito, R. Krichevsky, and A. Nicolis, Phys. Rev. A **96**, 033615 (2017).
[40] A. J. Groszek, D. M. Paganin, K. Helmerson, and T. P. Simula, arXiv:1708.09202.
[41] Y. V. Kartashov, B. A. Malomed, V. A. Vysloukh, M. R. Belić, and L. Torner, Opt. Lett. **42**, 446 (2017).
[42] S. Komineas, Eur. Phys. J. Spec. Top. **147**, 133 (2007).
[43] S. Xie, P. G. Kevrekidis, and T. Kolokolnikov, arXiv:1708.04336.